Journal of Magnetic Resonance 198 (2009) 94–104

Contents lists available at ScienceDirect

Journal of Magnetic Resonance

journal homepage: www.elsevier.com/locate/jmr

Simultaneous two-voxel localized ^{1}H-observed ^{13}C-edited spectroscopy for *in vivo* MRS on rat brain at 9.4 T: Application to the investigation of excitotoxic lesions

Bich-Thuy Doan [a,b,*], Gwennhael Autret [a], Joël Mispelter [c], Philippe Méric [a], William Même [d], Céline Montécot-Dubourg [d], Jean-Loup Corrèze [a], Frédéric Szeremeta [b], Brigitte Gillet [a], Jean-Claude Beloeil [b]

[a] *Laboratoire de RMN biologique, ICSN-CNRS, UPR, 2301, Avenue de la Terrasse, 91198 Gif sur Yvette cedex, France*
[b] *Laboratoire d'IRM et SRM des milieux vivants, CBM, CNRS, UPR 4301, Rue Charles Sadron, 45071 Orléans, cedex, France*
[c] *INSERM Unité 759, Institut Curie - recherche, Laboratoires R. Latarjet CU Bat 112, 91405 Orsay cedex, France*
[d] *Université d'Orléans, Laboratoire de Neurobiologie, UPRES-EA 2633 BP 6759, 45 067 Orléans cedex, France*

ARTICLE INFO

Article history:
Received 6 June 2008
Revised 21 January 2009
Available online 25 January 2009

Keywords:
^{1}H–(^{13}C) localized MRS
POCE-STEAM
POCE-PRESS
Hadamard encoding
Cerebral energy metabolism
[U–^{13}C] glucose injection

ABSTRACT

^{13}C spectroscopy combined with the injection of ^{13}C-labeled substrates is a powerful method for the study of brain metabolism *in vivo*. Since highly localized measurements are required in a heterogeneous organ such as the brain, it is of interest to augment the sensitivity of ^{13}C spectroscopy by proton acquisition. Furthermore, as focal cerebral lesions are often encountered in animal models of disorders in which the two brain hemispheres are compared, we wished to develop a bi-voxel localized sequence for the simultaneous bilateral investigation of rat brain metabolism, with no need for external additional references.

Two sequences were developed at 9.4 T: a bi-voxel ^{1}H–(^{13}C) STEAM-POCE (Proton Observed Carbon Edited) sequence and a bi-voxel ^{1}H–(^{13}C) PRESS-POCE adiabatically decoupled sequence with Hadamard encoding. Hadamard encoding allows both voxels to be recorded simultaneously, with the same acquisition time as that required for a single voxel. The method was validated in a biological investigation into the neuronal damage and the effect on the Tri Carboxylic Acid cycle in localized excitotoxic lesions. Following an excitotoxic quinolinate-induced localized lesion in the rat cortex and the infusion of U–^{13}C glucose, two ^{1}H–(^{13}C) spectra of distinct ($4 \times 4 \times 4$ mm^3) voxels, one centred on the injured hemisphere and the other on the contralateral hemisphere, were recorded simultaneously. Two ^{1}H bi-voxel spectra were also recorded and showed a significant decrease in *N*-acetyl aspartate, and an accumulation of lactate in the ipsilateral hemisphere. The ^{1}H–(^{13}C) spectra could be recorded dynamically as a function of time, and showed a fall in the glutamate/glutamine ratio and the presence of a stable glutamine pool, with a permanent increase of lactate in the ipsilateral hemisphere.

This bi-voxel ^{1}H–(^{13}C) method can be used to investigate simultaneously both brain hemispheres, and to perform dynamic studies. We report here the neuronal damage and the effect on the Tri Carboxylic Acid cycle in localized excitotoxic lesions.

1. Introduction

In vivo ^{13}C NMR spectroscopy associated with the administration of ^{13}C-labelled substrates is a powerful tool for the non-invasive investigation of brain metabolism. ^{13}C spectroscopy is the most appropriate method for monitoring the dynamics of metabolism in the Krebs cycle flux after the injection of substrates bearing labelled carbon atoms. In small animals, this method was first developed in 1985 with direct ^{13}C acquisition [1,2], and subsequently with localization, with and without ^{1}H decoupling [3–5]. In 1992, the first chemical shift imaging (CSI) experiment on the rat brain was performed with direct detection of ^{13}C [6].

Despite yielding a well-resolved ^{13}C spectrum with good chemical shift dispersion, the low sensitivity of the ^{13}C nucleus and the need for highly localized measurements in a functionally heterogeneous organ such as the brain have hampered the development of such methods, particularly for the study of small animals using small voxels localized on specific brain lesions. In addition to the development of high magnetic fields, a localized ^{13}C-edited sequence with ^{1}H acquisition is therefore of great interest, as it would have the same sensitivity as a ^{1}H sequence. In 1990, a ^{1}H-detected ^{13}C spectroscopic study using the POCE sequence [5], allowed the transfer of ^{13}C between glucose and glutamate to be

* Corresponding author. Present address: Laboratoire d'IRM et SRM du petit animal, CBM, CNRS, UPR 4301, Rue Charles Sadron, 45 071 Orléans Cedex, France. Fax: +33 2 38 63 15 17.
E-mail address: doan@cnrs-orleans.fr (B.-T. Doan).

1090-7807/$ - see front matter © 2009 Published by Elsevier Inc.
doi:10.1016/j.jmr.2009.01.023

visualized in the brain of a living rat. Sequences exploiting the indirect detection of ^{13}C, such as HMQC (2D) in 1993 [7] or POCE (1D) in 1999 [8], were combined with imaging sequences to obtain brain metabolite maps. In 1999, Pfeuffer et al. [9] developed a ^{13}C indirect localized spectroscopic method, using a sequence known as "adiabatic carbon editing and decoupling" (ACED) stimulated echo acquisition mode (STEAM), to study rat brain metabolism. In 2000, Watanabe et al. [10] combined a 2D HSQC sequence with 3D localization to study monkey brain metabolism after injection of [1-^{13}C] glucose.

Hadamard spectroscopic imaging (HSI) [11] allows the simultaneous acquisition of multiple slices or voxels and was proposed for reducing acquisition times in *in vivo* multi-slice or multi-voxel spectroscopic imaging. In 1995, Gonen et al. [12] combined a ^{1}H-decoupled phosphorus sequence with CSI and HSI to obtain spectroscopic images of four slices of human brain. Adding a PRESS localization sequence to a ^{1}H sequence already combined with CSI and HSI, enabled Dreher et al., working with healthy rat brain (1994) [13], and Gonen et al., working with human brain (1997) [14], to study four-voxel CSI spectra (HSI + PRESS). In 2001, Delmas et al. [15] showed that a ^{1}H COSY (2D) sequence combined with Hadamard encoding was suitable for studying brain metabolism of healthy or ischemic rat brain. This sequence was then used to study the focal excitotoxicity induced by ouabain in neonatal rats [16]. This simultaneous two-voxel method is therefore very useful in studying disorders occurring in only one of the cerebral hemispheres. When investigating a dynamic phenomenon, the simultaneous measurement of spectra from both voxels is more accurate than recording them successively and makes it unnecessary to administer a second ^{13}C labeled injection, thus saving an expensive substrate. We could follow changes of metabolism in an injured area, and compare it, simultaneously, to the contralateral voxel. This makes Hadamard encoding particularly suitable for use in studying this type of focal disorder.

The aim of our work was to combine two-voxel localization with a heteronuclear carbon sequence and proton acquisition. We created two sequences: POCE-STEAM and POCE-PRESS, suitable for simultaneous bilateral investigations of cerebral metabolism. This mode of acquisition allows one voxel to be used as the reference for the other. Spatial encoding using the excitation of two-frequency bands was performed by Hadamard encoding, in such a manner that the total acquisition time was the same as that required for a single-voxel experiment. This two-voxel localized ^{1}H-observed ^{13}C-edited spectroscopy is appropriate for investigating metabolic changes affecting the cerebral hemispheres differentially; a situation that is often encountered. In this work, it was developed and tested for small laboratory animals (rats).

2. Materials and methods

All experiments were conducted in accordance with French and European Community guidelines for the care and use of experimental animals, and under French Ministry of Agriculture permit no 91–164.

2.1. Two-voxel localized ^{1}H-observed ^{13}C-edited spectroscopy sequences

To enable us to select only ^{1}H nuclei bonded to the ^{13}C nuclei, we used an X filter with a POCE or ACED sequence [8,9], also known as the Xω [17] module. These filters refocus the $^{1}H(-^{13}C)$ proton magnetization with a spin-echo and the alternating application of a 180° ^{13}C pulse. Addition of the acquisitions recorded with and without the 180° ^{13}C pulse removes signals from $^{1}H(-^{12}C)$ systems, and only the $^{1}H(-^{13}C)$ magnetization remains.

2.1.1. POCE-STEAM sequence

The first sequence was based on the POCE-STEAM or ACED-STEAM module [9], and is presented in Fig. 1a. For the X filter, an adiabatic 180° WURST carbon pulse [18] was applied every two acquisitions during T_M.

2.1.2. POCE-PRESS sequence

A second $^{1}H-(^{13}C)$ localized sequence was developed based on PRESS ^{1}H localization [19], and using the same $^{1}H-(^{13}C)$ editing scheme as above (Fig. 1b). For the X filter, an adiabatic 180° WURST carbon pulse [18] was applied every two acquisitions during the second PRESS 180° proton pulse. The second echo time Te2 was equal to $1/J_{CH}$.

2.1.3. Bi-voxel mode

To record the two-voxel spectra, we used second order Hadamard encoding [11] performed after modifying the pulse corresponding to the chosen direction of the bi-voxel. Hadamard encoding has been proposed to perform multi-voxel localization. Signal information is encoded on the spins *n* times according to the rows (or columns) of a Hadamard matrix Hn of order *n*. This is accomplished by applying a shaped RF pulse in the presence of a field gradient. After storage of the *n* signals, the Hadamard transform gives the desired localized information $Fx(t)$: $Hn \cdot \mathbf{F}x(t) = \mathbf{S}n(t)$, *n* fid. Here, we used a low second order Hadamard matrix. The pulse was replaced by a double frequency excitation pulse used to define two voxels corresponding, in our case, to the two hemispheres of a rat brain. The acquisition was performed in two steps using two different bi-frequency pulses. A first FID (A) was recorded from the two voxels using a bi-frequency pulse with the same phases, and a second FID (B) was recorded with opposite phases. FIDs A and B were

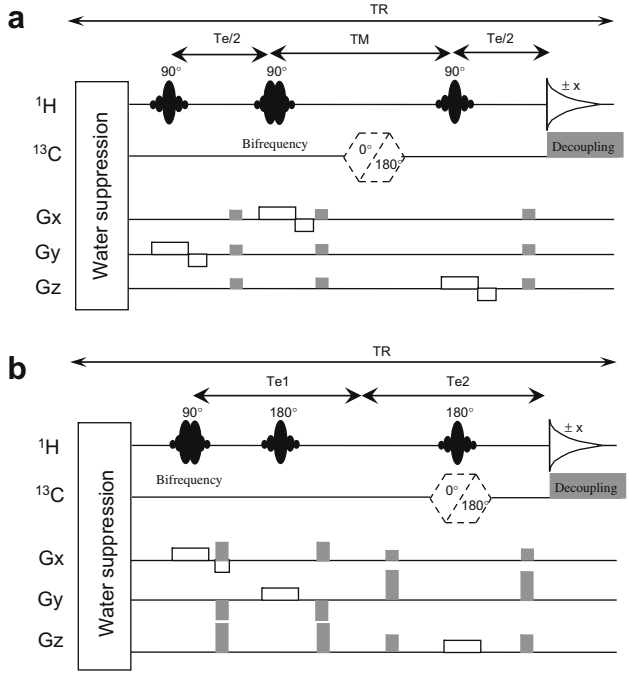

Fig. 1. (a) POCE sequence with two-voxel STEAM localization. TE was set to $1/J_{CH}$ and a 5 ms adiabatic WURST inversion pulse was applied during TM every two acquisitions. Adiabatic ^{13}C decoupling using WURST40 pulses was applied during acquisition, resulting in a 20 kHz decoupling bandwidth. A double frequency 90° pulse was used to select the two voxels. Refocussing gradients are indicated by small rectangles and spoiling gradients are displayed in grey. (b) POCE sequence with two-voxel PRESS localization. Te2 was set to $1/J_{CH}$. The same ^{13}C parameters as for STEAM were used. The bi-voxel localization was performed by a double frequency 90° pulse. The refocussing gradient is indicated in a small rectangle and spoiling gradients are displayed in grey.

added to obtain the FID corresponding to one of the voxels. They were then subtracted to obtain the FID corresponding to the other voxel. This is equivalent to data multiplication by the Hadamard matrix (see Eq. (1)).

$$H_2 = \begin{bmatrix} + & + \\ + & - \end{bmatrix} \quad (1)$$

Thus, the two spectra for the two voxels were simultaneously acquired without increasing the duration of the experiment, and with the same sensitivity as a single voxel acquisition. Hadamard encoding saves time, and also makes it possible to track and compare metabolism in two voxels simultaneously. Furthermore, this simultaneous acquisition has the advantage to include by design its own internal reference.

2.2. MRI-MRS experimental conditions

MR experiments were carried out at 9.4 T on a horizontal imaging spectrometer fitted with a ultra-shielded refrigerated 94/20 magnet (Bruker Biospec, Wissembourg, France) with an available diameter bore of 12 cm and equipped with a 200 mT/m actively shielded gradient coil.

Custom-made RF probes were home designed and built. The RF probes were composed of two concentric copper circular surface coils isolated by Teflon film: the first ($Ø_{int}$ = 23 mm) was used for ^{1}H excitation and reception, and the second ($Ø_{int}$ = 32 mm) for ^{13}C excitation.

An additional stand was built for the stereotaxic positioning of the head of the animals by means of a tooth bar and two ear bars, which provided volatile anaesthesia via a face mask, and maintained the body temperature at 37 °C by means of a circulating hot water bed.

The POCE-STEAM and POCE-PRESS sequences were implemented using Paravision 3.2 Bruker software. Hermitian pulses (1 ms) corresponding to an excitation bandwidth of 5700 Hz, were used. The bifrequency pulses were generated using Xwinnmr shape tool. The voxels were separated by 8310 Hz from their centrums (i.e. ±3 mm = 6 mm). Water suppression was performed using the VAPOR scheme [20].

In the POCE-STEAM and POCE-PRESS sequence, the T_E was chosen to edit the full ^{13}C magnetization (Te1 = Te2 = T_E = 1/J_{CH}). T_E = 7.9 ms was used, which was appropriate for the $J_{CH} \approx 127$ Hz values of aspartate (Asp), creatine (Cr), glutamine (Gln), glutamate (Glu), and lactate (Lac). TM was fixed at 20 ms and TR at 3 s throughout all the experiments. Adiabatic decoupling of ^{13}C nuclei was applied throughout the entire acquisition time of 128 ms. A WURST40 ^{13}C decoupling scheme was used *in vivo*. The total carbon bandwidth was 20 kHz, corresponding to 267 ppm. The ^{13}C channel decoupling power was 0.78 W. (2.93 W/kg). International guidelines recommend a maximum SAR over the head of 3 W/kg [21].

2.2.1. In vivo experiments

Gradient echo multi-slice, 1mm thickness, transversal images were recorded to delineate the injury volume, and to centre the ipsilateral voxel on the injury area. A global 10 × 4 × 4 mm voxel was defined to shim and to optimize water suppression. The Fastmap method [22] was performed combined with additional linear shimming steps. The resulting water line-width was about 12 Hz. Fine water suppression using the VAPOR sequence [20] was positioned before the localization sequence. Due to our surface coils, each voxel was limited to 4 × 4 × 4 mm (64 μL), and separated by 2 mm. The bi-voxel ^{1}H and ^{1}H–^{13}C POCE-PRESS sequences were used.

The acquisition time was 35 min. For dynamic recordings, consecutive spectra were recorded for a total accumulation time of about 2.5 h.

2.3. Animal preparation

The ^{1}H–(^{13}C) sequences were tested by investigating an excitotoxic lesion in the cortex/hippocampus of the left cerebral hemisphere of rats. Lesions were produced by the intra-cerebral administration of quinolinate four days before the measurements. Quinolinate (120 mM) circulated (5 μl/min for 40 min) through two implanted microdialysis probes (∅ = 0.5 mm, 4 mm efficient length) into the left cerebral hemisphere. The microdialysis method is based on natural liquid diffusion through a membrane to bring a molecule in situ with no physical damage, a 200 μl volume circulated into the probe allowing quinolinate to be softly administered by dialysis. The first probe was implanted at bregma −2 mm, 1 mm lateral; the second at bregma −4 mm, 3 mm lateral, in the cortico-hippocampus area.

The tests were carried out on six Wistar male adult rats (weighing between 220 and 280 g) anaesthetized with 1% isoflurane in 50% O_2 and 50% N_2O. Physiological parameters were monitored. The body temperature of the rats was measured during the experiment by means of a rectal thermo-sensor. A femoral venous line was implanted for the injection of [U–^{13}C] D-glucose at 5.3 g/kg. (99%, Cambridge Isotope Laboratories, Inc. via Eurisotop, CEA Saclay France), 3 M, in heparinated (5000 IU/l) physiological saline. A bolus of 317 mg glucose was injected during the first minute, followed by glucose infusion (5 min at 40 μl/min, 50 min at 30 μl/min, 100 min at 20 μl/min, and then 10 μl/min for the remaining time), which resulted in stable plasma glucose concentrations of about 20 mM, 30 min after injection. After the initial 10 min of infusion, the MRS experiment was started.

2.4. Quantification of in-vivo spectra

The *in-vivo* spectra were analyzed using the spectra simulation software, JMRUI 3 (http://www.mrui.uab.es/mrui/mrui_Overview.shtml, [23] AMARES) [24]. The prior knowledge database is the metabolites peaks database from Pfeuffer et al., the soft constraints for the line-width was 10–50 Hz, the frequency shift was inferior to ±10 Hz. Standard deviation errors were calculated by the fitting of the peaks. The spectra were zero-filled, with one level of zero-filling to 4 K for ^{1}H spectra and to 2 K for ^{1}H–^{13}C spectra, with exponential line broadening of 3 and 5 Hz, respectively, prior to Fourier transform.

2.5. Histology protocol

The histopathological consequences were investigated four days after injection of quinolinate. The ipsilateral side was compared to the un-injected contralateral side. Anesthetized rats (n = 6) were perfused with saline solution followed by a fixing solution. The brains were removed, kept in the same cold fixative solution, cryo-protected and then frozen in isopentane. Coronal 20-μm-thick brain sections were cut from the hippocampus at 1.8, 2.8, 3.8 and 4.8 mm behind the bregma using a cryomicrotome (Leica CM3050S).

2.5.1. Nissl staining

The sections were stained with Cresyl Violet and examined by conventional microscopy at ×100 magnification. The observer evaluated the severity of neuronal damage on four sections from each brain. The damage was defined on the basis of the following morphological characteristics: pycnotic nuclei, shrunken perikarya, micro-vacuolation, absence of cellular bodies, and presence of cellular debris in CA1, CA2, CA3, CA4 pyramidal cell layers and dentate gyrus granule cells layers of the hippocampus, and evaluated using a 4-point assessment scale: 0 for no change, 1 for slight change, 2 for moderate change and 3 for severe change.

2.5.2. GFAP immunohistochemistry

Immunohistochemical methods for the localization of glial fibrillary acidic protein (GFAP), which is a marker for astrocytes, were used to determine the extent of changes in sections adjacent to those used for the Nissl-stained procedure. Sections were first rinsed with PBS. Next, after incubating in PBS containing 0.4% normal goat serum (NGS) and 0.15% Triton X-100 and 1% bovine serum albumin (BSA), the sections were incubated overnight at 4 °C with an anti-Glial fibrillar acidic protein (GFAP) polyclonal rabbit antibody in PBS containing 0.4% NGS and 0.15% Triton X-100. For each brain, one section was incubated without the primary antibody to check the specificity of the anti-GFAP labelling. The sections were then rinsed with PBS and incubated with goat anti-rabbit FITC-labelled antibody. Sections were rinsed with 0.1% BSA in PBS. The sections were finally cover-slipped.

GFAP immunofluorescent labelling was quantified by determining the brightness-area-product (BAP) using the technique described by Smith et al. [25] in the CA1 and CA3 radiatum stratum of the hippocampus. Images were acquired digitally on a fluorescence microscope at X200 magnification. Photographs were taken with identical parameters. Each observed surface was 0.14 mm^2. Images were imported into Image J software (http://rsb.info.nih.gov/ij/ Wayne Rasband, NIH, USA), where the BAP was calculated. The BAP is defined by the formula: (Mean pixel brightness in range − Minimum pixel brightness in range) × (Number of pixels in range). The minimum brightness corresponds to the background, which is attributed mainly to non-specific binding of secondary antibody and the autofluorescence of the tissues.

2.6. Statistical analysis

For the lesion scores, a non-parametric Mann–Whitney test was used to compare the injected ROI chosen to be the hippocampus with the non-injected, contralateral hippocampus.

For the GFAP immunofluorescent labelling, a paired Student *t*-test was used to compare injured hippocampus with contralateral hippocampus.

A value $p < 0.05$ was considered as significant. All values are expressed as means ± standard error of the mean (SEM).

3. Results

3.1. Phantom experiments

The POCE ^{1}H–(^{13}C) localized sequence was first optimized *in vitro*. Using several phantoms of ^{13}C acetate in solution, the two-voxel POCE-STEAM sequence was optimized to find suitable ^{13}C and decoupling pulses as follows.

The ^{13}C 180° pulse was optimized using the POCE-STEAM scheme on a 50 mM ^{13}C acetate sample in D_2O. We compared adiabatic 180° pulses such as IBURP, SECH, and WURST to a classical square pulse (Fig. 2) with the criteria of sensitivity, bandwidth, B1 inhomogeneity robustness. The signal-to-noise ratio for the various pulses obtained after adjustment of the pulse power to maximize the signal, are compared in Table 1. The results clearly demonstrate that the adiabatic ^{13}C WURST 180° pulse was the most sensitive and efficient, since ^{1}H–^{13}C signal intensity was maximal over a large B1 power bandwidth. This pulse shape is also known to have the advantage to be less sensitive to B1 field inhomogeneity [18] and was chosen for all further measurements using the POCE-^{1}H scheme. The efficiency of the ^{1}H–(^{13}C) filter was demonstrated with a phantom consisting of 10 mM [1,2]^{13}C acetate and 10 mM creatine in 2.5% agarose gel. More than 99% of the ^{1}H–(^{13}C) signal was edited (Fig. 3).

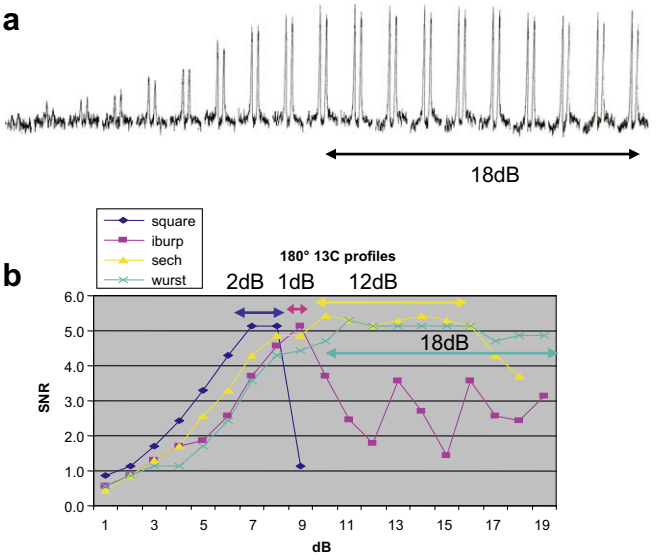

Fig. 2. The 2 dB step power variation of the ^{13}C pulse enabled RF field inhomogeneity effects to be simulated and intensity profiles for different 180° pulses to be generated over the pulse power in 2 dB steps. Square pulse length was 100 μs whereas adiabatic pulses lengths were 5 ms (a) WURST pulse. (b) $^{1}H(-^{13}C)$ signal intensity profiles for SQUARE, IBURP, SECH and WURST 180° pulses.

Table 1
Signal-to-noise ratio of different pulses determined to choose the more appropriate ^{13}C 180° pulse.

Pulse shape	Signal-to-noise ratio (SNR)
Square	4.8
IBURP	10.3
SECH	10.6
WURST	11.7

Decoupling schemes such as WALTZ [26], MLEV [27], GARP [28] and WURST40 [18], were tested to assess and control their decoupling bandwidth and efficiency. GARP and WURST40 gave the best results in terms of decoupling bandwidth on a 50 mM ^{13}C acetate sample in D_2O (Fig. 4). The WURST40 decoupling bandwidth was broader (1.5 fold), and its profile was more square than the GARP decoupling bandwidth. Indeed, because the WURST40 scheme is composed of adiabatic pulses, this decoupling scheme was less sensitive to B_1 field inhomogeneity than the GARP sequence. The decoupling power used was also lower (1.4 fold). Thus, it is clear that WURST40 decoupling is best suited for use in *in vivo* experiments.

After a first test on a water/oil sample, the two-voxel sequence was tested on a phantom consisting of two compartments or tubes in 2.5% agarose gel; one tube was filled with 20 mM creatine and the other with 20 mM lactate. A bi-frequency pulse was computed to obtain two 2.5 × 3 × 3.5 mm voxels 2 mm apart. One of the voxels was placed in the tube containing the lactate, and the other in the tube containing the creatine. The spectra obtained with the bi-frequency pulse, before (a,b) and after (c,d) multiplying the data by the Hadamard matrix are shown in Fig. 5. The two resulting spectra (c,d) correspond obviously to the spectrum corresponding to each individual voxel with no contamination of signal from the other voxel. Thus, the bi-frequency pulse has been demonstrated to be efficient and Hadamard encoding for simultaneous two-voxel excitation shown to be feasible in ^{1}H spectroscopy using our RF and experimental conditions.

The choice of the STEAM or PRESS localization sequence was based on the resulting experimental sensitivity obtained

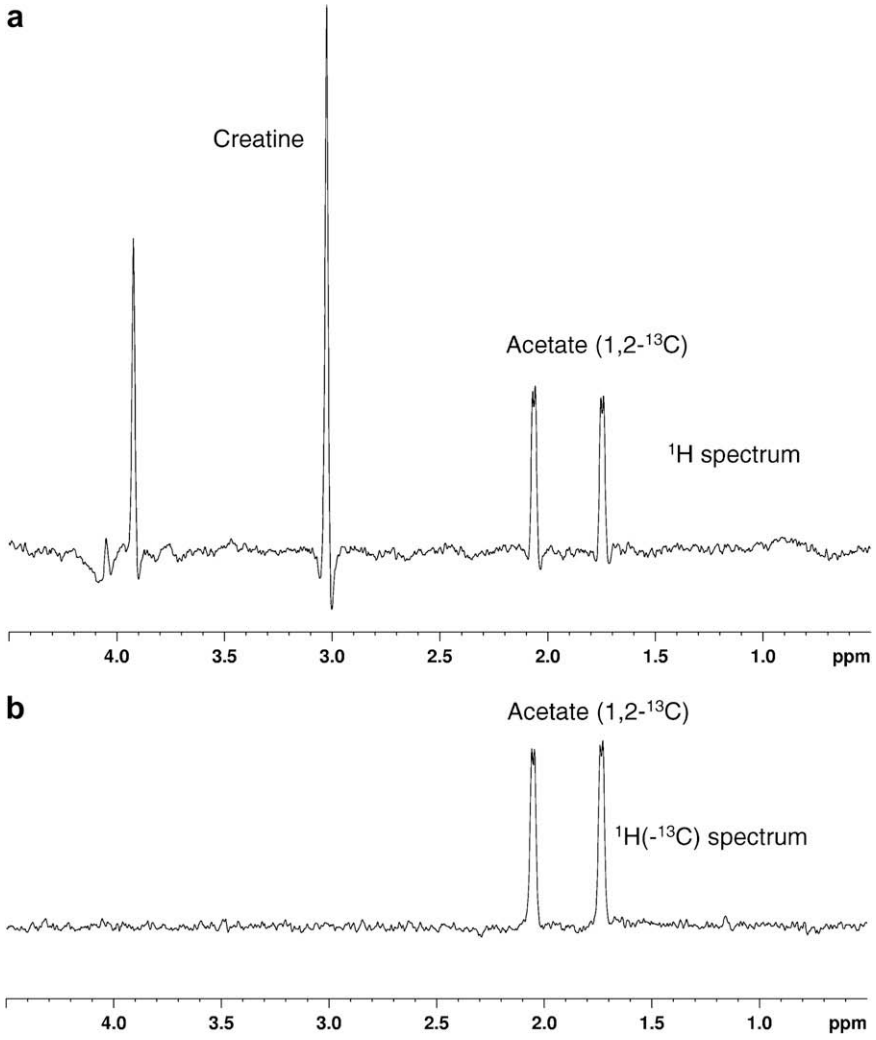

Fig. 3. POCE-^{1}H sequence tested on ^{13}C acetate + creatine in agarose gel showing the efficacy of the 1H–(^{13}C) filter spectrum (b) compared with ^{1}H spectrum (a). The figures are plotted with the same scale.

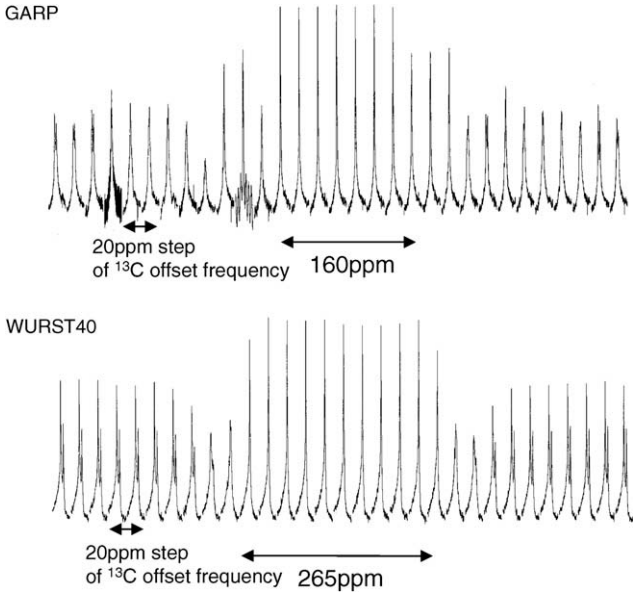

Fig. 4. A ^{13}C irradiation profile is displayed for decoupling modules: GARP and WURST40. Xω scheme was employed. The figure displays the acetate ^{1}H–(^{13}C) 'decoupled' peaks as a ^{13}C offset frequency in steps of 20 ppm. The decoupling should be efficient over a 200 ppm ^{13}C bandwidth.

previously. In theory, the PRESS sequence is twice as sensitive as STEAM, because the former corresponds to a spin-echo signal and the latter to a stimulated echo signal. The STEAM sequence is more robust to B_1 field inhomogeneity, as the voxel is defined by three 90° pulses. In practice, both sequences display similar sensitivity with a B1 inhomogeneous surface coil, the PRESS signal performs about 40% better. The expected two-fold increase in sensitivity of the PRESS sequence is not achieved in vitro due to 180° RF pulse imperfections (even with adiabatic pulses), and T_2 relaxation during the double spin-echo. Both sequences can therefore be used with a surface coil to perform bi-voxel experiments, but PRESS has a slight advantage.

3.2. In-vivo experiments

The injured brain side was first checked using T_2-weighted multi-slice SE images (Fig. 6a). The injury forms an edema that is visible as a hyper-signal located on the left side of the image, corresponding to the left side of the rat brain. On these images, a large 10 × 4 × 4 mm ROI was chosen. Two distinct 4 × 4 × 4 mm voxels (64 μL each) were generated by the bi-frequency pulse, such that the first voxel was centred on the lesion and the second was located symmetrically relative to the brain midline (Fig. 6a). The injured area occupied 68 ± 5% of the voxel. It should be pointed out that the voxels were separated by 2 mm (Fig. 6b), since an

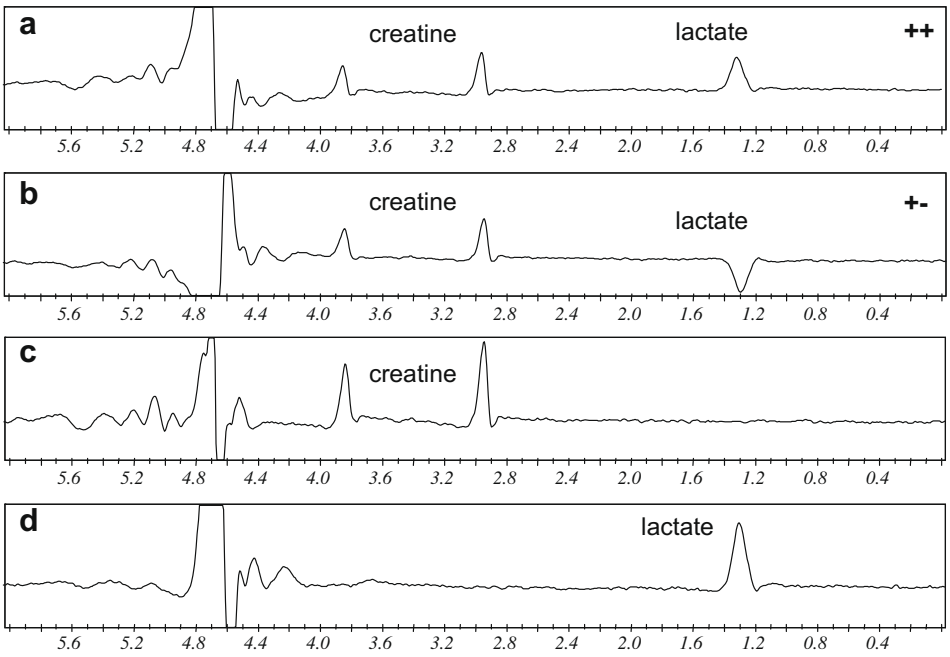

Fig. 5. Two-voxel POCE sequence tested on 10 mM lactate/creatine double compartment sample. As a consequence of the bi-frequency pulse, the two Hadamard spectra were obtained: one using the bi-frequency pulse with the same phases (a), the other using the bi-frequency pulse with opposite phases (b). The addition (c) and subtraction (d) spectra correspond to the spectra from each voxel.

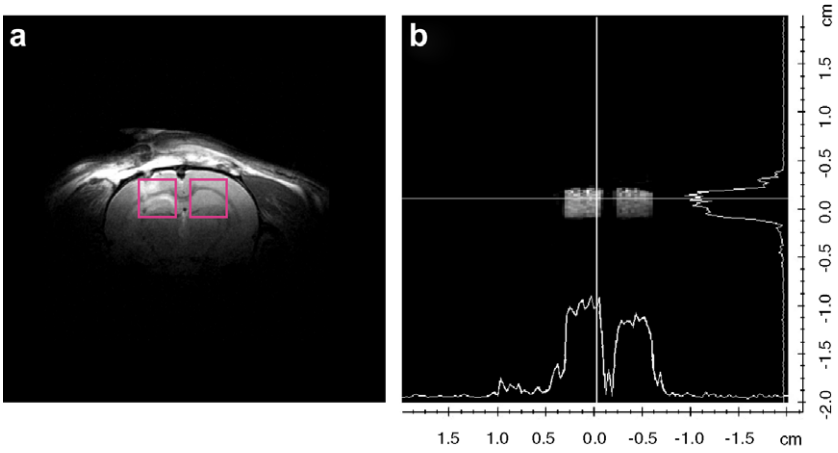

Fig. 6. (a): The two voxels position in a T_2-weighted image of transversal slice through the rat brain. The injured region is located in the left side of the brain. (b): MRI of the localized volumes selected by the two-voxel experiment with projections in the x and y directions.

intervoxel distance of 50% of the voxel size allows any spatial contamination to be avoided.

3.2.1. ^1H results

An ^{1}H spectrum was recorded in each hemisphere using a two-voxel ^{1}H sequence to test the cerebral disruption in a static manner. It should be noted that measured water line-widths were identical for the ipsilateral and contralateral voxels, and since the T_2 values did not depend on the lesions, the excitotoxicity being one of the main different processes involved in the ischemic lesions [29], the MRS integration of the peaks can be considered as quantitative. Peaks were assigned following recommendations by de Graaf [30]. The spectral resolution resulting from the 9.4 T magnetic field made possible the separation of the glutamate peak (2.35 ppm) from the glutamine peak (2.45 ppm) (Fig. 7a and 7b). The integration of the doublet of the lactate methyl group (Lac, 1.32 ppm) was performed by deconvolution of the superimposed macromolecular peaks (MM). It should be noted that it is estimated that only 70% of the lactate pool is detected by NMR [31].

The comparison between the spectra recorded from the contralateral and ipsilateral cerebral hemispheres revealed differences in metabolite levels. In the ipsilateral hemisphere, the ^{1}H spectra ($n = 6$) showed a significant lower level of NAA (2.01 ppm, mean $S = 9.8 \pm 3.5$ to 5.2 ± 2, i.e. factor -1.9, $p < 0.05$) as well as a relative accumulation of lactate (1.32 ppm, $S = 2.2 \pm 2$ to 11.1 ± 5, i.e. factor 5, $p < 0.01$). The standard deviation of the noise was similar in each spectrum.

The glutamate (Glu, 2.34 ppm) level was significantly lower ($S = 3.9 \pm 1$ to 2.1 ± 1, i.e. factor 1.9, $p < 0.03$). The glutamine, (Gln, 2.45 ppm), phosphorus-creatine/creatine pool (PCr–Cr, 3.02 ppm), choline residue (rCho, 3.21 ppm) and taurine (Tau, 3.42 ppm) levels showed no significant changes. The myo-inositol (Ins,

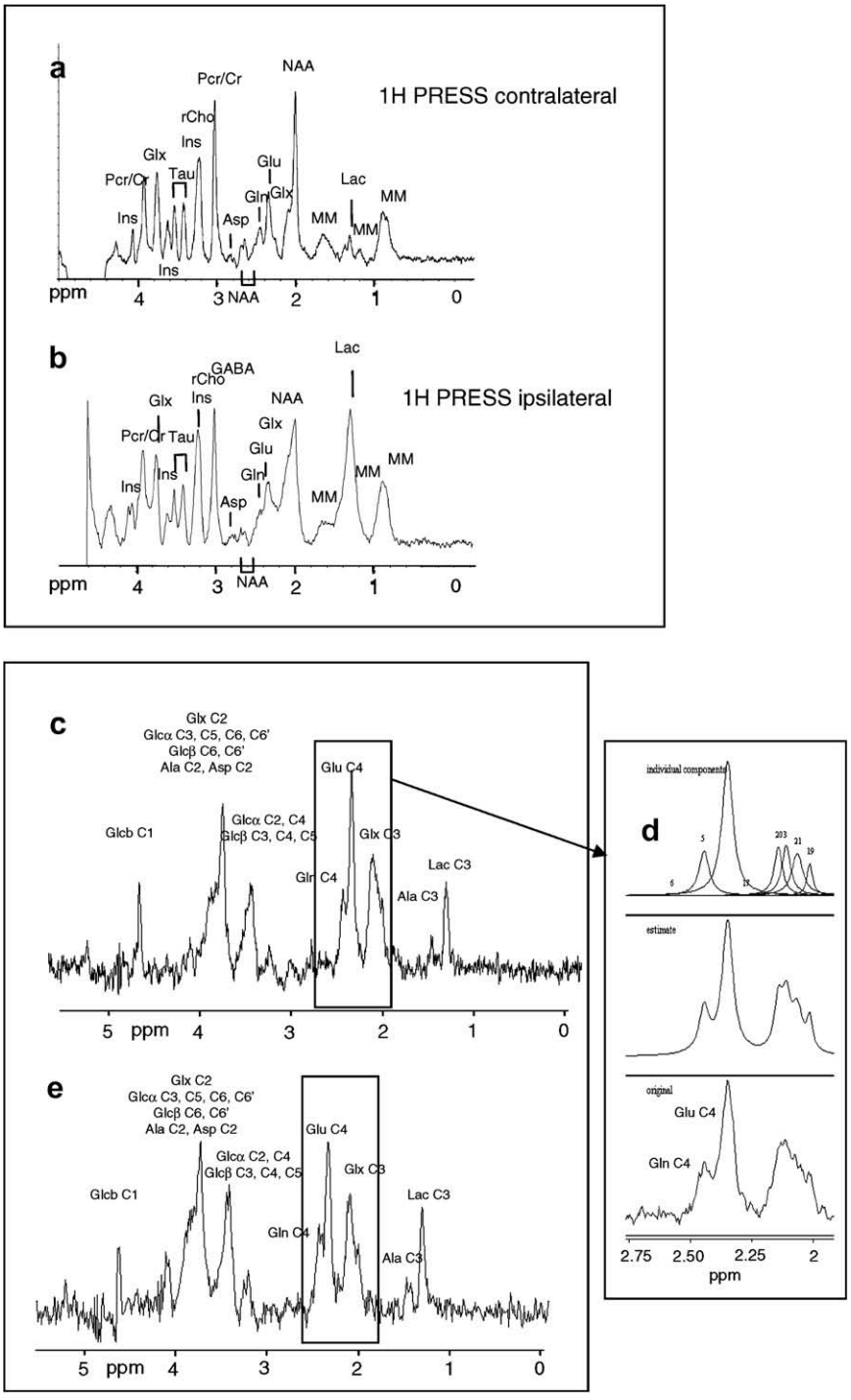

Fig. 7. (a) and (b): Reference ^{1}H spectra of the voxels in each cerebral hemisphere of the rat brain acquired at 9.4 T, using PRESS localization and VAPOR water suppression. (a): Contralateral voxel. (b): Ipsilateral voxel. The ^{1}H spectrum was recorded with, T_E = 15 ms, TR = 3 s, number of experiments = 128, number of points = 4096, spectrum width = 4000 Hz, total time = 8 min. The processing consisted of zero filling to 8192 points and 3 Hz exponential line broadening before Fourier transform. (c), (d) and (e): ^{1}H($-^{13}$C) spectra of the two voxels in each cerebral hemisphere of the rat brain acquired at 9.4 T, using two-voxel POCE-PRESS sequence and VAPOR water suppression. (c): Contralateral voxel. (d): Zoomed region of the ^{1}H($-^{13}$C) spectrum of the contralateral voxel showing the Glu–Gln C4 fitting. (e): Ipsilateral voxel. The recording parameters are Te1 = Te2 = 7.9 ms, TR = 3 s, number of experiments = 128 × 2, number of points = 1024, spectrum width = 4000 Hz, acquisition every 35 min for a total time = 2 h 38 min. The processing consisted of zero filling to 2048 points and 5 Hz exponential line broadening.

3.53 ppm) level is higher ($S = 1.2 \pm 0.5$ to 2.3 ± 0.9, factor 1.9, $p < 0.07$). The contribution of choline (rCho) resonances located close to this Ins peak are negligible, as insignificant changes in choline peaks were observed. The relative lipid (CH3, 0.9 ppm) level also increased significantly ($S = 5.62 \pm 5$ to 11 ± 5, i.e. by a factor of 1.96, $p < 0.05$).

3.2.2. $^{1}H(-^{13}C)$ results

After the two-voxel ^{1}H sequence, the two-voxel ^{1}H($-^{13}$C) POCE-PRESS sequence was carried out *in vivo*. Protons were observed bound to ^{13}C in various metabolites resulting from [U-^{13}C] glucose consumption in the TCA cycle. According to the literature [9], we abbreviated as in the literature [9] the peak labels of the ^{1}H-de-

tected carbon positions, e.g., GlnC4 represents glutamate containing a ^{13}C at position C4.

The sensitivity of $^{1}H(-^{13}C)$ spectra ($n = 6$) made possible the quantitative acquisition of the spectra every 35 min. It was possible to discriminate between the Gln and Glu C4 peaks during the continuous infusion of glucose (Fig. 7c and 7d), and to quantify Gln C4, Glu C4, Glx C3, Lac C3, Ala C3, Asp C3, Glc αC1 Glc C4 βC3-5 at various times during the TCA cycle by peak simulation. The sensitivity of the $^{1}H-(^{13}C)$ spectra was sufficient to follow the dynamic pattern of the Lac C3, Glu C4, Gln C4, Glc αC1, Glc C4 βC3-5 peaks during the injection of ^{13}C glucose.

After 1 h 10 min, the Gln C4 ipsi/contra ratio was stable (1 ± 0.17), and Glu C4 was found to have decreased significantly (factor 2 ± 0.11, $p < 0.05$). The instantaneous production of lactate significantly increased in the ipsilateral hemisphere (factor 1.7 ± 0.3, $p < 0.05$) (Fig. 8). This increase was smaller than that observed in the ^{1}H spectra.

With regard to the dynamic change observed over 2.2 h, on the contralateral side, we observed a similar change in labelled Glu and Gln resonances, with a progressive increase in ^{13}C-labelling for about 70 min, followed by a stable plateau during the observation period. The contralateral versus ipsilateral comparison showed that the change in ^{13}C Gln resonance labelling was similar in both hemispheres, with an increase occurring during the observation period followed by a drop, corresponding to the decrease in the the level of ^{13}C-labelled glucose infused. This suggested that astrocytes activity remained similar, at least for this metabolic pathway, even though reactive astrocytes (GFAP+) are present in the ipsilateral side (Fig. 9). For Glu and Lac labelling, we observed very different changes in the two voxels. The rate of production of Glu C4 was lower in the ipsilateral side, and was at its peak value 185 min after the beginning of infusion at a level four times lower than that reached in the contralateral side. The level of Lac C3 rose for 70 min, to reach a maximum level that was 2.5 times higher than that in the contralateral hemisphere. The decrease in Glu production rate highlighted the fact that the capacity of neurons to produce glutamate had been severely disrupted and/or the ability of neurons to transform glutamine into glutamate was impaired due to the neuronal lesion (Fig. 9).

3.3. Histology

3.3.1. Neuropathological changes

The contralateral hippocampus displayed little or no damage (scores near 0). Four days after quinolinate injection, severe disruption of the cytoarchitecture was observed in the CA1, CA2,

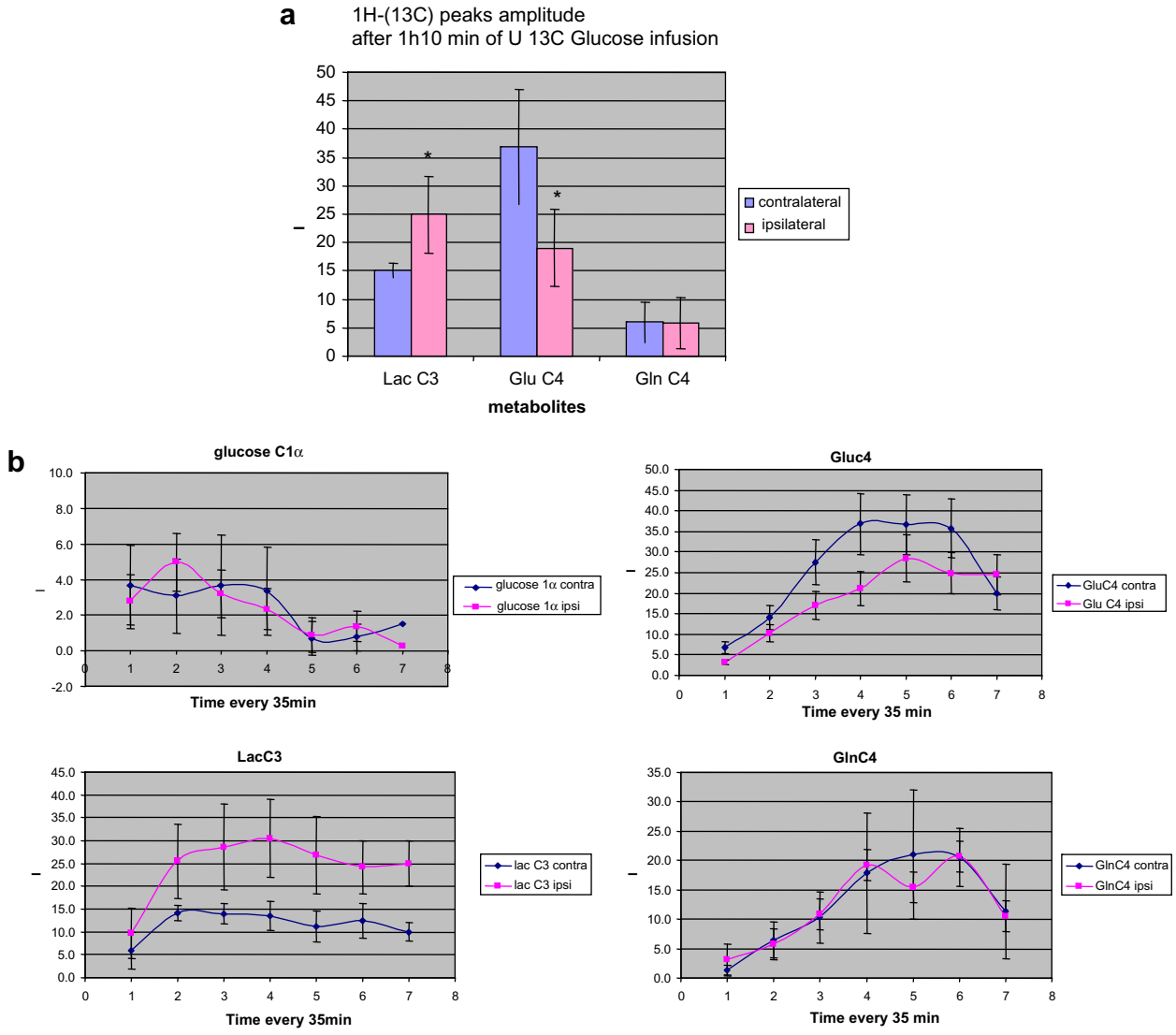

Fig. 8. Comparison of the metabolite signals between contralateral voxel and ipsilateral voxel measured by $^{1}H(-^{13}C)$ bi-voxel MRS. (a) Values 1 h after U–^{13}C glucose administration. (b) Time course of Lac, Glucose, Gln and Glu peaks after ^{13}C glucose administration.

CA3, CA4 pyramidal and dentate gyrus granule cell layers of the ipsilateral hippocampus. The damage score of each pyramidal cell layer subfield was significantly higher in the ipsilateral hippocampus than in the contralateral hippocampus (Table 2). At −1.8 and −2.8 mm from bregma, the pyramidal cell layers had almost completely degenerated (Fig. 9), and the dentate gyrus granule cell layer was virtually non-existent at −1.8 mm from bregma.

3.3.2. Glial fibrillary acidic protein immunohistochemistry

Four days after quinolinate injections, the brightness-area-product was significantly higher in the ipsilateral than in the contralateral hippocampus (Table 3). BAP values indicated that the expression level for GFAP was higher in astrocytes in the ipsilateral hippocampus. GFAP-positive cells appeared as a dense radial network, spreading throughout the whole thickness of the CA1 and CA3 stratum radiatum (Fig. 9).

4. Discussion

4.1. In-vivo dynamic ^{1}H–^{13}C experiments at 9.4T

We were able to quantify and compare simultaneously the signals from both cerebral hemispheres *in-vivo*, one ipsilateral, the other contralateral, in a dynamic manner. The volume of each voxel was 64 μL. We were able to record quantitative data in a period of 35 min. Pfeuffer et al. [9] used the ACED-STEAM sequence on a healthy rat at 9.4 T. on a voxel containing most of the brain; the size of the voxel was 137 μl and the spectrum was obtained within 15 min. To achieve equivalent sensitivity, at the same field, using the 2.14-fold smaller voxel of our study, we should have needed to accumulate data for 4.6 times longer. In fact, using the POCE-PRESS sequence we accumulated the data for only 2.1 times longer and achieved sufficient sensitivity to analyze our spectra quantitatively.

4.2. ^{1}H acquisition versus ^{13}C acquisition

We opted for ^{1}H rather than ^{13}C acquisition in order to benefit from its greater sensitivity. A 1D version of HSQC (with voxel localization) or a HMQC (with slice selection) could have been employed, but these inverse detection sequences have several disadvantages that render them unsuitable. With successive polarization transfers, we could theoretically have obtained 64 times more signal in comparison to direct ^{13}C observation ($S/B = (\gamma^{1}H/\gamma^{13}C)^{3}$) [32]. However, for *in vivo* experiments it is inadvisable to use numerous pulses, due to problems associated with pulse angle imperfections which lead to a loss of signal, especially when using a surface coil. A DEPT localized non ^{1}H decoupled sequence has been described by Deelchand et al. [4] who recorded 400 μl voxel spectra of rat brain *in vivo* within 5 min, thus demonstrating the feasibility of using this dedicated method to study the human brain at a very high magnetic field. For small animals at 9.4 T, it proved simpler to implement the POCE localized 4-pulse sequence, and to compute the simplified ^{1}H–(^{13}C) spectra with ^{1}H detection. We therefore preferred to use a $^{1}H(-^{13}C)$ sequence with ^{1}H acquisition, the sensitivity of the resulting signal then being that sensitivity of the proton.

4.3. In vivo biological MRS ^{1}H and ^{1}H–^{13}C results are consistent with impairment of the neuronal metabolism and/or neuronal death, and dysfunction of the TCA cycle

Intra-cerebral administration of quinolinic acid (QA) is commonly used in animal models of cerebral injuries in Huntington's disease (HD) [33–35]. Biochemical, histological and behavioural studies of the QA model of HD have been performed previously over a wide range of doses (from 30–500 nmol QA) and time-scales (minutes to several months) [36–39].

Our non-invasive MRS tool should allow longitudinal follow-up and monitoring of the disease as well as of recovery. The probes used to inject QA were small enough (diameter 0.5 mm) not to cause any serious mechanical damage, as had been demonstrated by previous MRI experiments [40] and as observed in the histology data, in which only minor damage could be detected. Several hours after the implantation and the perfusion of the fibre by mock CSF, only a narrow strip around the tractus of the fibre exhibited hyperintensity suggesting deleterious processes were active in the area concerned (data not shown). However, this area is quite negligible in size compared to those showing evidence of edema after quinolinate administration. It therefore seems highly unlikely that the changes observed in the spectra were due to fibre implantation. Though the voxel recorded for MRS contained cortical and hippocampal ROIs where the neuronal damage had occurred, detailed histological analysis was limited to the dorsal hippocampus to allow a more reliable comparison of the quantitative analysis of the histological data from the ipsilateral and contralateral hemispheres.

Our ^{1}H spectra matched those of Tkác et al. [41]. They explored the model using ^{1}H spectroscopy and recorded a similar set of data post injection (after five days). A decrease in NAA observed revealed severe impairment of the neuronal metabolism and/or neuronal death. A decrease in glutamate demonstrated severe functional impairment of neurons. Simultaneously, the stable amount of glutamine associated with the activated/proliferative feature of astrocytes within the lesion observed by histology would indicate that the astrocytes were activated or well-preserved. In the injured tissues, the fall in glutamate ^{13}C labelling could be compensated for by an accumulation of glutamine ^{13}C labelling related to a blockade of neuronal glutamine–glutamate inter-conversion, and the conversion of glutamate into glutamine by glutamine synthase in astrocytes. There was a greater increase in the amount of lactate (×5) in the ^{1}H spectra in both hemispheres, compared to ^{1}H–(^{13}C) spectra (×1.7). The ^{1}H Lactate pool reflects the difference between the production of lactate and its consumption by oxidation and washout. The ^{1}H–(^{13}C) lactate signal reflects lactate production. Our ^{1}H, and especially our ^{1}H–(^{13}C) MRS, data suggest that we may not only have detected passive lactate from a necrotic area. Our ^{1}H–(^{13}C) MRS data suggest long-term lactate production by a non-negligible proportion of cells, for example activated astrocytes, as it is known that glycolysis in the astrocytes favours lactate production [42,43]. The ^{1}H information on the accumulated lactate may therefore only indicate an imbalance between the production, consumption and clearing of lactate before measurement, whereas $^{1}H(-^{13}C)$ provides real-time, dynamic information on metabolic changes in the injured tissue.

4.4. Hadamard simultaneous bi-voxel encoding is advantageous for biological studies

In view of the dynamic approach provided by the POCE ^{1}H–(^{13}C) localized sequence, multi-voxel measurements using Hadamard encoding make it possible to record spectra from the control cerebral hemisphere at the same time as the injured hemisphere, thus providing an internal reference from the same rat and in the same time required for a single-voxel experiment. The two-voxel strategy is therefore an efficient method of recording voxels *in vivo* simultaneously [13] on rat brain, as demonstrated in previous 2D COSY experiments studying ischemia or brain tumors [15] and in our present work. For multi-voxel recording, a CSI sequence could obviously be used. However, this sequence would lack sensitivity and would not have been suitable for the dynamic follow-up of

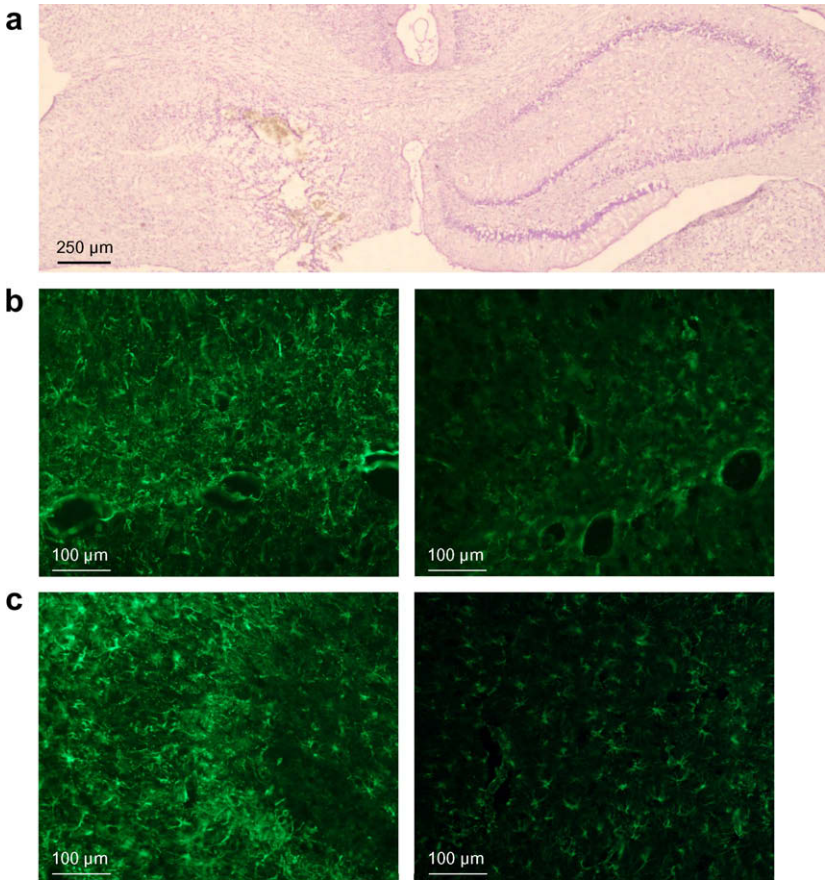

Fig. 9. Histology of coronal section at −2.8 mm from bregma, four days after unilateral quinolinate injection (the injected side is on the left). (a) Cresyl violet staining (magnification ×20). On the non-injected side there is no damage. On the injected side, pyramidal cells and dentate gyrus granule cells layers have completely degenerated. (b) GFAP immmunoreactivity in the CA1 stratum radiatum (magnification ×200). (c) GFAP immmunoreactivity in the CA3 stratum radiatum (magnification ×200). Note the dense radial network of GFAP positive cells in the injected hippocampus.

Table 2
Semi-quantitative evaluation of the damage in the CA1, CA2, CA3, CA4 pyramidal cells layers and in the dentate gyrus granule cells layers of the left hippocampus, four days after unilateral quinolinate injection.

Coronal sections (mm from bregma)	CA1	CA2	CA3	CA4	Dentate gyrus
−1.8	3 ± 0*				2.83 ± 0.16*
−2.8	2.83 ± 0.16*	3 ± 0*	3 ± 0*	3 ± 0*	2 ± 0.34*
−3.8	2.41 ± 0.49*	2.75 ± 0.17*	2.33 ± 0.44*	3 ± 0*	2.08 ± 0.37*
−4.8	2 ± 0.54*(dorsal)	1.6 ± 0.51*	0.9 ± 0.55	1.9 ± 0.50*	1.9 ± 0.53*

Scale: 0 indicates no cell death, grade 1, <10% damaged neurons, grade2, 10–50% damaged neurons; grade 3, >50% damaged neurons. Each score shows the severity of the changes.
* $p < 0.05$ vs non-injected side.

Table 3
Quantitative evaluation of GFAP immunofluorescent labelling in CA1 and CA3 stratum radiatum (SR) of the hippocampus four days after unilateral quinolinate injection.

Coronal sections (mm from bregma)	CA1 SR quinolinate-injected side	CA1 SR non-injected side	CA3 SR quinolinate injected side	CA3 SR non-injected side
−1.8	10.3 ± 2.5	3.8 ± 3.4		
−2.8	66.1 ± 25*	9.7 ± 7.2	84.9 ± 26.2*	7.7 ± 5.1
−3.8	52.3 ± 24.4*	8.9 ± 5.3	28.4 ± 8.8*	6.9 ± 3.3
−4.8	66.6 ± 19.8*(dorsal)	19.5 ± 10.9 (dorsal)	26.1 ± 8.8	21.3 ± 15.5

GFAP immunofluorescent labelling was quantified by determining the brightness-area-product (BAP). BAP is expressed ($\times 10^6$).
* $p < 0.05$ vs non-injected side. Note the strong GFAP immunoreactivity in the injected hemisphere.

the TCA cycle every 35 min. In case of the type of focal injury that is often encountered, the bi-voxel strategy is a powerful alternative, allowing sensitivity to be optimized.

4.5. Further developments to increase sensitivity

The sensitivity and resolution of the method could be increased further by building homogeneous coils. This would allow the observation of regions within the brain other than the superficial cortex or hippocampus, as required for other pathological models. It would also allow the voxel size to be increased so that larger lesions could be used to avoid a partial volume effect. Homogeneous coils would also permit more homogeneous excitation pulses, thus optimizing the sensitivity. Multi-channel excitation could also prove useful for delineating the injury and avoiding partial volume effects.

5. Conclusion

The two-voxel ^{1}H-observed ^{13}C-edited localized spectroscopy sequence can be used to record highly sensitive localized spectra

on rat brain *in vivo*. It also makes it possible to investigate simultaneously the metabolism in both cerebral hemispheres, so that each voxel provides the other with an intrinsic signal reference, in order to detect neuronal damage (decreased NAA level) and impairment of the TCA cycle (permanent lactate 13C labelling production, decrease in glutamate 13C labelling and stable levels of glutamine 13C labelling) in localized excitotoxic lesions. The fact that lactate is produced by a non-negligible proportion of cells in the damaged hemisphere four days after lesion initialization, could be used as the basis for therapeutic intervention.

Both ^{1}H localized STEAM and PRESS sequences combined with ^{13}C edition can be used.

Acknowledgments

Dr. G. Autret thanks the 'Ministère de la Recherche et Technologies' for PhD funding, and the authors thanks Dr. M. Ghosh, Dr. Andrew Atkinson and Dr. Stéphane Petoud for editorial support. We are also grateful to Dr. D. Wecker (Bruker) for his valuable help and discussion in programming the ^{1}H–(^{13}C) sequence.

References

[1] D.L. Rothman, K.L. Behar, H.P. Hetherington, J.A. den Hollander, M.R. Bendall, O.A. Petroff, R.G. Shulman, 1H-Observe/13C-decouple spectroscopic measurements of lactate and glutamate in the rat brain in vivo, Proc. Natl. Acad. Sci. USA 82 (6) (1985) 1633–1637.
[2] N.R. Sibson, A. Dhankhar, G.F. Mason, K.L. Behar, D.L. Rothman, R.G. Shulman, In vivo ^{13}C NMR measurements of cerebral glutamine synthesis as evidence for glutamate-glutamine cycling, Proc. Natl. Acad. Sci. USA 94 (6) (1997) 2699–26704.
[3] R. Gruetter, G. Adriany, I.Y. Choi, P.G. Henry, H. Lei, G. Oz, Localized in vivo 13C NMR spectroscopy of the brain, NMR Biomed. 16 (6–7) (2003) 313–338.
[4] D.K. Deelchand, K. Ugurbil, P.G. Henry, Investigating brain betabolism at high fields using localized ^{13}C NMR spectroscopy without ^{1}H decoupling, Magn. Reson. Med. 55 (2006) 279–286.
[5] S.M. Fitzpatrick, H.P. Hetherington, K.L. Behar, R.G. Shulman, The flux from glucose to glutamate in the rat brain *in vivo* as determined by ^{1}H-observed, ^{13}C-edited NMR Spectroscopy, J. Cereb. Blood Flow Metab. 10 (1990) 170–179.
[6] S. Morishita, M. Sumi, R. Nishimura, M. Takahashi, N. Iriguchi, Carbone-13 chemical shift imaging of [1-^{13}C] glucose under metabolism in the rat head *in vivo*, Radiat. Med. 10 (1992) 94–100.
[7] P.C. van Zijl, A.S. Chesnick, D. Despres, C.T. Moonen, J. Ruiz-Cabello, P. van Gelderen, *In vivo* proton spectroscopy and spectroscopic imaging of [1-^{13}C]-glucose and its metabolic products, Magn. Reson. Med. 30 (1993) 544–551.
[8] F. Hyder, R. Renken, D.L. Rothman, *In vivo* carbon-edited detection with proton echo-planar spectroscopic imaging (ICED PEPSI):[3,4-$^{13}CH_2$] glutamate/glutamine tomography in rat brain, Magn. Reson. Med. 42 (1999) 997–1003.
[9] J. Pfeuffer, I. Tkác, I-Y. Choi, H. Merkle, K. Ugurbil, M. Garwood, R. Gruetter, Localized *in vivo* ^{1}H NMR detection of neurotransmitter labeling in rat brain during infusion of [1-^{13}C] D-glucose, Magn. Reson. Med. 41 (1999) 1077–1083.
[10] H. Watanabe, Y. Ishihara, K. Okamoto, K. Oshio, T. Kanamatsu, Y. Tsukada, 3D localized ^{1}H-^{13}C heteronuclear single-quantum coherence correlation spectroscopy *in vivo*, Magn. Reson. Med. 43 (2000) 200–210.
[11] L. Bolinger, J.S. Leigh, Hadamard spectroscopic imaging (HSI) for multivolume localization, J. Magn. Reson. 80 (1988) 162–167.
[12] O. Gonen, J. Hu, R. Stoyanova, J.S. Leigh, G. Goelman, T.R. Brown, Hybrid three dimensional (1D-Hadamard, 2D-Chemical Shift Imaging) phosphorus localized spectroscopy of phantom and human brain, Magn. Reson. Med. 33 (1995) 300–308.
[13] W. Dreher, D. Leibfritz, Double-echo multislice proton spectroscopic imaging using Hadamard slice encoding, Magn. Reson. Med. 31 (1994) 596–600.
[14] O. Gonen, F. Arias-Mendoza, G. Goelman, 3D localized *in Vivo* ^{1}H spectroscopy of human brain by using a hybrid of 1D-Hadamard with 2D-chemical shift imaging, Magn. Reson. Med. 37 (1997) 644–650.
[15] F. Delmas, J-C. Beloeil, B.P.J. van der Sanden, K. Nicolay, B. Gillet, Two-voxel localization sequence for *in Vivo* two-dimensional homonuclear correlation spectroscopy, J. Magn. Reson. 149 (2001) 119–125.
[16] W.B. Veldhuis, M. van der Stelt, F. Delmas, B. Gillet, G.A. Veldink, J.F. Vliegenthart, K. Nicolay, P.R. Bar, In vivo excitotoxicity induced by ouabain, a Na+/K+-ATPase inhibitor, J. Cereb. Blood Flow Metab. 23 (1) (2003) 62–74.
[17] G. Otting, H. Senn, G. Wagner, K. Wüthrich, Editing of 2D ^{1}H NMR spectra using X half-filters. Combined use with residue-selective 15N labeling of proteins, J. Magn. Reson. 70 (1986) 500–505.
[18] E. Kupce, R. Freeman, Adiabatic pulses for wideband inversion and broadband decoupling, J. Magn. Reson. Ser. A 115 (1995) 273–276.
[19] P.A. Bottomley, Selective volume method for performing localized NMR spectroscopy, US Patent 4480228, 1984
[20] I. Tkác, Z. Starcuk, I.-Y. Choi, R. Gruetter, *In vivo* ^{1}H NMR spectroscopy of rat brain at 1 ms echo time, Magn. Reson. Med. 41 (1999) 649–656.
[21] Criteria for significant risk investigations of magnetic resonance diagnostic devices-guidance for industry and FDA staff, FDA, Center of Devices and Radiological Health, 2003. Available from: http://www.fda.gov/cdrh/ode/guidance/793.html.
[22] R. Gruetter, Automatic, localized in vivo adjustment of all first- and second-order shim coils, Magn. Reson. Med. 29 (1999) 804–811.
[23] A. Naressi, C. Couturier, J.M. Devos, M. Janssen, C. Mangeat, R. de Beer, D. Graveron-Demilly, Java-based graphical user interface for the MRUI quantitation package, MAGMA 12 (2001) 141–152.
[24] L. Vanhamme, A. van den Boogaart, S. Van Huffel, Improved method for accurate and efficient quantification of MRS data with use of prior knowledge, J. Magn. Reson. 129 (1997) 35–43.
[25] P.D. Smith, K.J. Mc Lean, M.A. Murphy, Y. Wilson, M. Murphy, A.M. Turnley, M.J. Cook, A brightness-area-product-based protocol for the quantitative assessment of antigen abundance in fluorescent immunohistochemistry, Brain Res. Protoc. 15 (1) (2005) 21–29.
[26] A.J. Shaka, J. Keeler, R. Freeman, Evaluation of a new broadband decoupling sequence: WALTZ 16, J. Magn. Reson. 53 (1983) 313–340.
[27] M. H Levitt, R. Freeman, Composite pulse decoupling, J. Magn. Reson. 43 (1981) 502.
[28] A.J. Shaka, P.B. Barker, R. Freeman, Computer-optimized decoupling scheme for wideband applications and low-level operation, J. Magn. Reson. 64 (1985) 547–552.
[29] A. van der Toorn, R.M. Dijkhuizen, C.A. Tulleken, K. Nicolay, T1 and T2 relaxation times of the major 1H-containing metabolites in rat brain after focal ischemia, NMR Biomed. 8 (6) (1995) 245–252.
[30] R.A. de Graaf, D.L. Rothman, *In vivo* detection and quantification of scalar coupled ^{1}H NMR resonances, Concept. Magn. Reson. 13 (1) (2001) 32–76.
[31] K. Kotitschke, K.D. Schnackerz, R. Dringen, U. Bogdahn, A. Haase, M. von Kienlin, Investigation of the ^{1}H NMR visibility of lactate in different rat and human brain cells, NMR Biomed. 7 (1994) 349–355.
[32] R.R. Ernst, G. Bodenhausen, A. Wokaun, Principles of Nuclear Magnetic Resonance in One and Two Dimensions, Clarendon Press, Oxford, 1987.
[33] R. Schwarcz, W.O. Whetsell, R.M. Mangano, Quinolinic acid: an endogenous metabolite that produces axon-sparing lesions in rat brain, Science 219 (1983) 316–318.
[34] M.F. Beal, N.W. Kowall, D.W. Ellison, M.F. Mazurek, K.J. Swartz, J.B. Martin, Replication of the neurochemical characteristics of Huntington disease by quinolinic acid, Nature 321 (1986) 168–171.
[35] M.F. Beal, R.J. Ferrante, K.J. Swartz, N.W. Kowall, Chronic quinolinic acid lesions in rats closely resemble Huntington disease, J. Neurosci. 11 (1991) 1649–1659.
[36] Y.M. Bordelon, M.F. Chesselet, M. Erecinska, I.A. Silver, Effects of intrastriatal injection of quinolinic acid on electrical activity and extracellular ion concentrations in rat striatum *in vivo*, Neuroscience 83 (1998) 459–469.
[37] Y.M. Bordelon, M.F. Chesselet, Early effects of intrastriatal injections of quinolinic acid on microtubule-associated protein-2 and neuropeptides in rat basal ganglia, Neuroscience 93 (1999) 843–853.
[38] G. Ceresoli-Borroni, P. Guidetti, R. Schwarcz, Acute and chronic changes in kynurenate formation following an intrastriatal quinolinate injection in rats, J. Neural Transm. 106 (1999) 229–242.
[39] F.V. Mena, P.J. Baab, C.L. Zielke, H.R. Zielke, *In vivo* glutamine hydrolysis in the formation of extracellular glutamate in the injured rat brain, J. Neurosci. 60 (2000) 632–641.
[40] J-L. Correze, P. Meric, A. Volk, J. Mispelter, J. Seylaz, Relation between diffusion MRI, 1H spectroscopic imaging and release of excitatory amino acids in focal excitotoxic lesions, J. Cereb. Blood Flow Metab. 15 (1990) 416.
[41] I. Tkác, C. Dirk Keene, J. Pfeuffer, W.C. Low, R. Gruetter, Metabolic changes in quinolinic acid-lesioned rat striatum detected non-invasively In Vivo ^{1}H NMR spectroscopy, J. Neurosci. Res. 66 (2001) 891–898.
[42] L. Pellerin, A.K. Bouzier-Sore, A. Aubert, S. Serres, M. Merle, R. Costalat, P.J. Magistretti, Activity-dependent regulation of energy metabolism by astrocytes: an update, Glia 55 (2007) 1251–1262.
[43] L. Hertz, L. Peng, G.A. Dienel, Energy metabolism in astrocytes: high rate of oxidative metabolism and spatiotemporal dependence on glycolysis/glycogenolysis, J. Cereb. Blood Flow Metab. 27 (2007) 219–249.